

Non-stoichiometry effects on the extreme magnetoresistance in Weyl semimetal WTe₂

J. X. Gong,^{1,2} J. Yang,¹ M. Ge,^{2,a)} Y. J. Wang,¹ D. D. Liang,¹ L. Luo,¹ X. Yan,¹ W. L. Zhen,¹ S. R. Weng,¹ L. Pi,^{1,2} W. K. Zhu,^{1,a)} and C. J. Zhang^{1,3,a)}

¹*High Magnetic Field Laboratory, Chinese Academy of Sciences, Hefei 230031, China*

²*Hefei National Laboratory for Physical Sciences at Microscale, University of Science and Technology of China, Hefei 230026, China*

³*Institute of Physical Science and Information Technology, Anhui University, Hefei 230601, China*

^{a)}Electronic addresses: gemin@mail.ustc.edu.cn, wkzhu@hmfl.ac.cn, and zhangcj@hmfl.ac.cn.

The extremely large non-saturated magnetoresistance is an unusual property of many semimetals, some of which have topological quantum states. In the present paper, the non-stoichiometry effect on the magnetoresistance is systematically investigated for the Weyl semimetal WTe₂. The as-grown samples have a slight difference in Te vacancies, whose magnetoresistance and Hall resistivity are measured and analyzed with a two-carrier model. The fitting results show that the extreme magnetoresistance is strongly dependent on the residual resistivity ratio, which is interpreted as the degree of non-stoichiometry and the ratio of electron-type and hole-type carriers. Such an electron-hole compensation mechanism is further confirmed by the measurements on the annealed samples with artificial Te vacancies. The non-stoichiometry effect is eventually understood in terms of electron doping which breaks the balance between electron-type and hole-type carriers. These facts demonstrate that the compensation effect is the dominant mechanism of the extreme magnetoresistance in WTe₂, in spite of other possible origins.

I. INTRODUCTION

Giant or colossal magnetoresistance (MR) is one of the most important properties in magnetic multilayers and manganites,^{1,2} in which the resistance changes significantly with applied magnetic field. Such a novel property can be utilized to make multifunctional devices, e.g., magnetic sensors,³ magnetic memory,⁴ hard drives,⁵ etc. While the materials with a colossal MR are mostly insulators or semiconductors, the MR in conventional metals is usually very small, showing quadratic field dependence in low fields and saturated in high fields.⁶ The extremely large and non-saturated positive

MR (XMR) has been recently discovered in a number of metals or semimetals, including Cd_3As_2 ,⁷ TaP ,⁸ WTe_2 ,⁹ PtSn_4 ,¹⁰ antimonides,¹¹⁻¹⁶ etc.^{17,18} Particularly, some of the XMR materials have been demonstrated or predicted to possess a topological semimetal state. For example, Cd_3As_2 is a three-dimensional Dirac semimetal,¹⁹ and WTe_2 is a type-II Weyl semimetal.²⁰

Different from the colossal MR effect, in which the carrier scattering from magnetic disorder and spin fluctuation is greatly suppressed under magnetic field,² various mechanisms are proposed to explain the XMR phenomena. In LaBi and LaSb , the XMR is attributed to the electron-hole compensation,²¹ which means a perfect balance between the electron and hole populations. For Cd_3As_2 and TaAs family, the large MR cannot be simply understood in terms of the compensation effect, and one proposed scenario is that the novel topological protection suppresses the backscattering at zero magnetic field.^{7,8} Spectroscopic evidence shows that the XMR in YSb is special, because YSb lacks both topological protection and electron-hole compensation.²² The large MR of PtSn_4 is associated with its ultrahigh mobility.¹⁰

Among these systems, WTe_2 is a unique one whose XMR shows no sign of saturation in the magnetic field even as high as 60 T.⁹ This discovery has triggered extensive researches to reveal its origin. Based on electronic structure calculation, the XMR in bulk WTe_2 is ascribed to the compensation between the electron and hole populations, which is supported by the angle-resolved photoemission spectroscopy (ARPES) results and the quantum oscillation experiments.^{23,24} Even though, other possible origins are proposed. A distinct reduction in electron density occurs below 50 K indicating a possible electronic structure change, which might be the direct driving force of the electron-hole compensation and the XMR as well.²⁵ The circular dichroism observed in another ARPES experiment suggests that the spin-orbit coupling and related spin and orbital angular momentum textures play an important role in the XMR.²⁶ Also, the charge compensation is highly dependent on sample thickness. The balance of electron and hole states is respected only when considering at least three Te-W-Te layers,²⁷ which may suggest other mechanisms in thin samples. Recently, a few experiments have attempted to find out the origin by gate-tuning the carrier density of a thin sample in situ.²⁸⁻³⁰ Until now, the origin of the XMR in WTe_2 is still under debate.

In this work, we try to check the compensation mechanism by comparing the samples with different Te vacancies (i.e., the non-stoichiometry effect), which are introduced during the natural

growth or annealing process. The as-grown samples have a slight difference in Te vacancies, whose MR and Hall resistivity are measured and analyzed with a two-carrier model. The fitting results show that the XMR is strongly dependent on the residual resistivity ratio (RRR), which is interpreted as the degree of non-stoichiometry and the ratio of electron-type and hole-type carriers. Such an electron-hole compensation mechanism is further confirmed by the measurements on the annealed samples with artificial Te vacancies. The non-stoichiometry effect is eventually understood in terms of electron doping which breaks the balance between electron-type and hole-type carriers. These facts demonstrate that the compensation effect is the dominant mechanism of the XMR in WTe₂, in spite of other possible origins.

II. EXPERIMENTAL METHODS

Single crystals of WTe₂ were grown with Te flux. In order to obtain samples of different qualities, source powders of tungsten and tellurium were prepared at a series of chemical ratios. The powder mixture was placed in an alumina crucible, with another crucible containing quartz wool mounted on top of it. Both crucibles were sealed in a silica ampoule, heated to 1000 °C and held for 10 hours, and then cooled down to 600 °C at a rate of 2 °C/h. The excess Te flux was removed by centrifugation at 600 °C. The crystal structure and phase purity were checked by single crystal X-ray diffraction (XRD) on a Rigaku-TTR3 X-ray diffractometer using Cu K α radiation, and the morphological characterization was performed on a Hitachi TM3000 scanning electron microscope (SEM). The chemical components of as-grown samples and annealed samples were obtained on an Oxford energy dispersive spectroscope (EDS). The MR and Hall measurements were taken on a home-built Multi Measurement System on a Janis-9T magnet.

III. RESULTS AND DISCUSSION

As seen in the SEM image in Fig. 1(a), the as-grown WTe₂ single crystal exhibits ribbon-like morphology with clean and shining surface. The single crystal XRD pattern shows only (0 0 2*l*) peaks [Fig. 1(b)], confirming that the naturally cleaved surface is the *ab* plane and the sample is a single phase, i.e., *Pmn*2₁ (31). Figure 1(c) illustrates the crystal structure, in which silver and orange spheres represent W and Te atoms, respectively. From Fig. 1(c), we find that WTe₂ adopts a typical crystal

structure of layered transition metal dichalcogenides (TMDs), namely, metal layer located between adjacent chalcogenide layers. Such sandwich sheets stack along the c axis, with van der Waals bonding between them. As a result of the strong anisotropy, WTe₂ is typically electronically two-dimensional. Moreover, another structural feature is present in WTe₂. The zigzag tungsten chains are formed along the a axis, making it structurally quasi-one-dimensional.

Figure 2(a) shows the temperature dependence of resistivity for the as-grown samples of different qualities, denoted by #1, #2, #3 and #4, respectively. As described above, these samples are grown from source powders at various ratios, although the EDS characterizations show that they all keep good chemical stoichiometry without any detectable difference. The sample quality can be roughly evaluated by the residual resistivity ratio (RRR), defined as the ratio of resistivity at room temperature and at 0 K, which is strongly depending on the amounts of impurities and defects. In the present paper, the RRR takes the value $\frac{\rho(250\text{ K})}{\rho(2\text{ K})}$. As shown in Fig. 2(a), all the samples exhibit a metallic behavior with a small resistivity. However, the RRR ranges from 113 to 272, reflecting different qualities of samples, i.e., the degree of non-stoichiometry.

The longitudinal MR ($\frac{\Delta\rho}{\rho_0} = \frac{\rho_H - \rho_0}{\rho_0}$) and Hall resistivity are further measured at 2 K under a magnetic field up to 9 T, with the current applied along the a axis and the magnetic field applied perpendicular to the ab plane. The extremely large MR is reproduced on our samples, e.g., about $1.6 \times 10^5\%$ at 9 T for sample #1. The XMR and Hall resistivity vary significantly for different samples. Namely, with the increase of RRR, the XMR and Hall resistivity (negative) become larger and larger. Such a positive correlation between RRR and XMR is consistent with previous report.³¹ If we note that the RRR reflects the sample quality and degree of non-stoichiometry, we can deduce that the larger XMR is corresponding to the better stoichiometry. In order to check the compensation effect on XMR, a two-carrier model (or two-band model) is used to fit the MR and Hall resistivity data and extract the density and mobility of carriers. In this model, the longitudinal resistivity ρ_{xx} and transverse resistivity ρ_{xy} are described as²⁵

$$\rho_{xx} = \frac{(n_e\mu_e + n_h\mu_h) + (n_e\mu_e\mu_h^2 + n_h\mu_e^2\mu_h)B^2}{e[(n_e\mu_e + n_h\mu_h)^2 + (n_h - n_e)^2\mu_e^2\mu_h^2B^2]}, \quad (1)$$

and

$$\rho_{xy} = \frac{(n_h\mu_h^2 - n_e\mu_e^2)B + \mu_e^2\mu_h^2(n_h - n_e)B^3}{e[(n_e\mu_e + n_h\mu_h)^2 + (n_h - n_e)^2\mu_e^2\mu_h^2B^2]} \quad (2)$$

where e is the electron charge, n is the carrier density, μ is the mobility, and the subscripts e and h refer to electron-type and hole-type carriers, respectively. According to the model, the condition for ρ_{xx} to increase as B^2 is $n_e = n_h$, which means that electrons and holes are perfectly compensated by each other. Moreover, this model also suggests that ρ_{xy} should be proportional to B , i.e., linearly field dependent, for the perfect compensation. Slight deviation from the perfect compensation will cause a nonlinear field dependence of Hall resistivity in high field region. A simple power-law fitting for sample #1 (which has the best quality) gives $MR \propto B^{1.77}$ [as shown in Fig. 2 (b)], as well as the nonlinear $\rho_{xy}(B)$ curves, suggesting that the samples are not in the perfectly compensated regime. Further fittings using the above equations result in the ratios n_e/n_h . Non-oscillatory curves in Fig. 2(c) represent the fitted curves, which agree well with the experimental data, showing sufficiently good fittings and reliable fitting results.

Figure 3(a) presents the MR and n_e/n_h as a function of RRR for all the as-grown samples, obtained from Fig. 2. It is easily found that with the increase in RRR and XMR, the ratio n_e/n_h gradually approaches the perfect compensation value, i.e., 1. That is to say, the dependence of XMR on the RRR can be indeed interpreted as the change of n_e/n_h . For a sample of higher quality, the less defects correspond to a larger RRR, and the more balanced n_e/n_h ratio gives rise to a larger XMR. Similar phenomenon has been found in the investigation on the temperature dependence of XMR.²⁵

Since the XMR is strongly dependent on the non-stoichiometry effect, artificial defects may be introduced to conduct more conclusive research work, considering that the naturally as-grown samples are very close to each other in stoichiometry but a distinct gradient of vacancies can be obtained by the annealing processes. Different time lengths of annealing in vacuum yield a series of non-stoichiometric samples, i.e., 0%, 5% and 10%. The percentages represent the degree of Te vacancies, setting the as-grown sample as 0%. Note that the three samples are cut from the same piece of as-grown sample. As shown in Figs. 4(a)-4(c), with the increase of Te vacancies, the RRR and XMR are greatly reduced. The degradation of sample quality indeed suppresses the XMR. In order to reveal the underlying information, again we fit the MR and Hall resistivity data with the two-carrier model. The resultant n_e/n_h ratios are plotted as a function of Te vacancies in Fig. 3(b), along with the XMR. We

can see that the introduced defects in the annealed samples indeed lead to a less compensated n_e/n_h , which is eventually responsible for the reduced XMR. The results obtained from the annealed samples are consistent with those from the as-grown samples.

Here we propose a possible scenario to explain the non-stoichiometry effect on the XMR in WTe₂. From the band structure calculations and quantum oscillation analyses,^{23,24} the Fermi surfaces can be generally described by the two-carrier model, i.e., one electron-like band and one hole-like band. As illustrated in Fig. 5(a), the band structures around the Fermi level are composed of one electron-type pocket and one hole-type pocket. When the electron-type carriers and hole-type carriers are completely compensated, which is also the stoichiometric case, the MR reaches its maximum value, according to the above equations. However, once the electron-type carriers and hole-type carriers become non-compensated, no matter what reason it is, the MR is reduced. In the present experiment, both the as-grown samples and the annealed samples have a certain degree of Te vacancies, i.e., electron doping. As seen in Fig. 5(b), the electron doping increases the Fermi level, which breaks the balance between electron-type carriers and hole-type carriers and leads to a reduction in MR. A further reasonable guess is that the opposite situation, i.e., the hole doping with the hole-type carriers exceeding the electron-type carriers, may also comply with this rule. Such a mechanism probably accounts for the XMR in WTe₂ and related materials,²¹ where the best sample (i.e., with the largest RRR) has a n_e/n_h ratio that is closest to the perfect compensation and thus the largest MR.

Before ending the present paper, we may talk more about the relationship between XMR and topological semimetal states. Although all the found topological semimetals seem to exhibit the XMR effect, the XMR does not necessarily lead to topological semimetal states. For some XMR materials like LaSb,¹² distinct trivial features are revealed by first-principles calculations and ARPES experiment.^{21,32} In such systems, the XMR may be only originating from the compensation effect, not relevant to any topological mechanism.

IV. CONCLUSIONS

In conclusion, the non-stoichiometry effect on the XMR is investigated for the Weyl semimetal WTe₂. The as-grown samples have a slight difference in Te vacancies, whose MR and Hall resistivity are measured and analyzed with a two-carrier model. The fitting results show that the XMR is strongly

dependent on the RRR, which is interpreted as the degree of non-stoichiometry and the n_e/n_h ratio. Such an electron-hole compensation mechanism is further confirmed by the measurements on the annealed samples with artificial Te vacancies. The non-stoichiometry effect is eventually understood in terms of electron doping which breaks the balance between electron-type and hole-type carriers. These facts demonstrate that the compensation effect is the dominant mechanism of the XMR in WTe_2 , in spite of other possible origins.

ACKNOWLEDGMENTS

This work was supported by the National Key R&D Program of China (Grant Nos. 2016YFA0300404 and 2017YFA0403600), the National Natural Science Foundation of China (Grant Nos. 51603207, U1532267, 11574288 and 11674327), and the Natural Science Foundation of Anhui Province (Grant No. 1708085MA08).

- ¹M. N. Baibich, J. M. Broto, A. Fert, F. N. Vandau, F. Petroff, P. Eitenne, G. Creuzet, A. Friederich, and J. Chazelas, *Phys. Rev. Lett.* **61**, 2472 (1988).
- ²M. B. Salamon and M. Jaime, *Rev. Mod. Phys.* **73**, 583 (2001).
- ³J. E. Lenz, *Proc. IEEE* **78**, 973 (1990).
- ⁴Y. Moritomo, A. Asamitsu, H. Kuwahara, and Y. Tokura, *Nature* **380**, 141 (1996).
- ⁵J. M. Daughton, *J. Magn. Magn. Mater.* **192**, 334 (1999).
- ⁶A. B. Pippard, *Magnetoresistance in Metals* (Cambridge University Press, Cambridge, 1989).
- ⁷T. Liang, Q. Gibson, M. N. Ali, M. Liu, R. J. Cava, and N. P. Ong, *Nat. Mater.* **14**, 280 (2014).
- ⁸C. Zhang, C. Guo, H. Lu, X. Zhang, Z. Yuan, Z. Lin, J. Wang, and S. Jia, *Phys. Rev. B* **92**, 041203 (2015).
- ⁹M. N. Ali, J. Xiong, S. Flynn, J. Tao, Q. D. Gibson, L. M. Schoop, T. Liang, N. Haldolaarachchige, M. Hirschberger, N. P. Ong, and R. J. Cava, *Nature* **514**, 205 (2014).
- ¹⁰E. Mun, H. Ko, G. J. Miller, G. D. Samolyuk, S. L. Bud'ko, and P. C. Canfield, *Phys. Rev. B* **85**, 035135 (2012).
- ¹¹O. Pavlosiuk, P. Swatek, and P. Wiśniewski, *Sci. Rep.* **6**, 38691 (2016).
- ¹²F. F. Tafti, Q. D. Gibson, S. K. Kushwaha, N. Haldolaarachchige, and R. J. Cava, *Nat. Phys.* **12**, 272 (2015).
- ¹³N. Wakeham, E. D. Bauer, M. Neupane, and F. Ronning, *Phys. Rev. B* **93**, 205152 (2016).
- ¹⁴Y. Wang, Y. Wang, C. Y. Xi, L. S. Ling, S. L. Zhang, L. He, T. Han, H. Han, J. Yang, D. Liang, J. Gong, L. Luo, W. Tong, L. Zhang, Z. Qu, Y. Y. Han, W. K. Zhu, L. Pi, C. Zhang, and Y. Zhang, e-print arXiv:1702.08121 [cond-mat.mtrl-sci].
- ¹⁵K. Wang, D. Graf, L. Li, L. Wang, and C. Petrovic, *Sci. Rep.* **4**, 7328 (2014).
- ¹⁶Y. Li, L. Li, J. Wang, T. Wang, X. Xu, C. Xi, C. Cao, and J. Dai, *Phys. Rev. B* **94**, 121115 (2016).
- ¹⁷S. Sun, Q. Wang, P.-J. Guo, K. Liu, and H. Lei, *New J. Phys.* **18**, 082002 (2016).
- ¹⁸N. Kumar, Y. Sun, N. Xu, K. Manna, M. Yao, V. Suss, I. Leermakers, O. Young, T. Forster, M. Schmidt, H. Borrmann, B. Yan, U. Zeitler, M. Shi, C. Felser, and C. Shekhar, *Nat. Commun.* **8**, 1642 (2017).
- ¹⁹Z. Wang, H. Weng, Q. Wu, X. Dai, and Z. Fang, *Phys. Rev. B* **88**, 125427 (2013).

- ²⁰A. A. Soluyanov, D. Gresch, Z. Wang, Q. Wu, M. Troyer, X. Dai, and B. A. Bernevig, *Nature* **527**, 495 (2015).
- ²¹P.-J. Guo, H.-C. Yang, B.-J. Zhang, K. Liu, and Z.-Y. Lu, *Phys. Rev. B* **93**, 235142 (2016).
- ²²J. He, C. Zhang, N. J. Ghimire, T. Liang, C. Jia, J. Jiang, S. Tang, S. Chen, Y. He, S. K. Mo, C. C. Hwang, M. Hashimoto, D. H. Lu, B. Moritz, T. P. Devereaux, Y. L. Chen, J. F. Mitchell, and Z. X. Shen, *Phys. Rev. Lett.* **117**, 267201 (2016).
- ²³I. Pletikoscic, M. N. Ali, A. V. Fedorov, R. J. Cava, and T. Valla, *Phys. Rev. Lett.* **113**, 216601 (2014).
- ²⁴Z. W. Zhu, X. Lin, J. Liu, B. Fauque, Q. Tao, C. L. Yang, Y. G. Shi, and K. Behnia, *Phys. Rev. Lett.* **114**, 176601 (2015).
- ²⁵Y. K. Luo, H. Li, Y. M. Dai, H. Miao, Y. G. Shi, H. Ding, A. J. Taylor, D. A. Yarotski, R. P. Prasankumar, and J. D. Thompson, *Appl. Phys. Lett.* **107**, 182411 (2015).
- ²⁶J. Jiang, F. Tang, X. C. Pan, H. M. Liu, X. H. Niu, Y. X. Wang, D. F. Xu, H. F. Yang, B. P. Xie, F. Q. Song, P. Dudin, T. K. Kim, M. Hoesch, P. K. Das, I. Vobornik, X. G. Wan, and D. L. Feng, *Phys. Rev. Lett.* **115**, 166601 (2015).
- ²⁷P. K. Das, D. Di Sante, I. Vobornik, J. Fujii, T. Okuda, E. Bruyer, A. Gyeenis, B. E. Feldman, J. Tao, R. Ciancio, G. Rossi, M. N. Ali, S. Picozzi, A. Yadzani, G. Panaccione, and R. J. Cava, *Nat. Commun.* **7**, 10847 (2016).
- ²⁸L. Wang, I. Gutierrez-Lezama, C. Barreteau, N. Ubrig, E. Giannini, and A. F. Morpurgo, *Nat. Commun.* **6**, 8892 (2015).
- ²⁹Y. Wang, K. Wang, J. Reutt-Robey, J. Paglione, and M. S. Fuhrer, *Phys. Rev. B* **93**, 121108 (2016).
- ³⁰V. Fatemi, Q. D. Gibson, K. Watanabe, T. Taniguchi, R. J. Cava, and P. Jarillo-Herrero, *Phys. Rev. B* **95**, 041410 (2017).
- ³¹M. N. Ali, L. Schoop, J. Xiong, S. Flynn, Q. Gibson, M. Hirschberger, N. P. Ong, and R. J. Cava, *EPL* **110**, 67002 (2015).
- ³²H. Oinuma, S. Souma, D. Takane, T. Nakamura, K. Nakayama, T. Mitsuhashi, K. Horiba, H. Kumigashira, M. Yoshida, A. Ochiai, T. Takahashi, and T. Sato, *Phys. Rev. B* **96**, 041120 (2017).

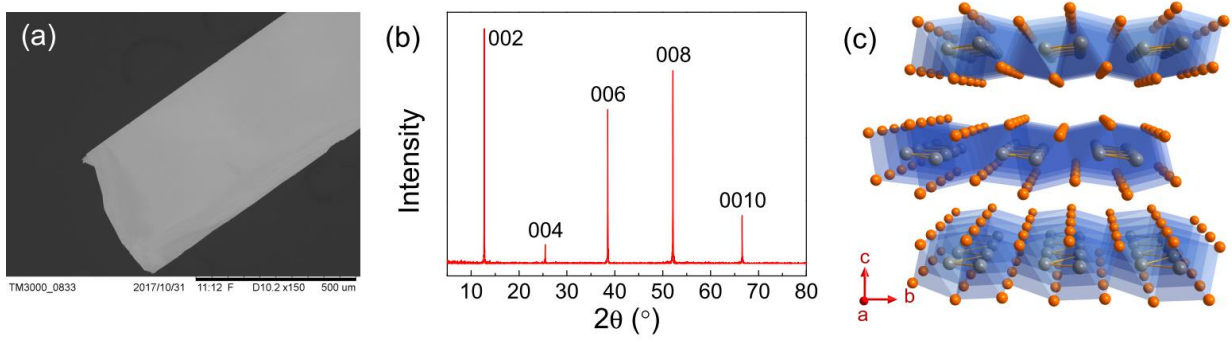


FIG. 1. (a) SEM image of WTe₂ single crystal. (b) Single crystal XRD pattern. (c) Crystal structure of WTe₂ along the *a* axis that is parallel to the W-W zigzag chains. Silver and orange spheres represent W and Te atoms, respectively.

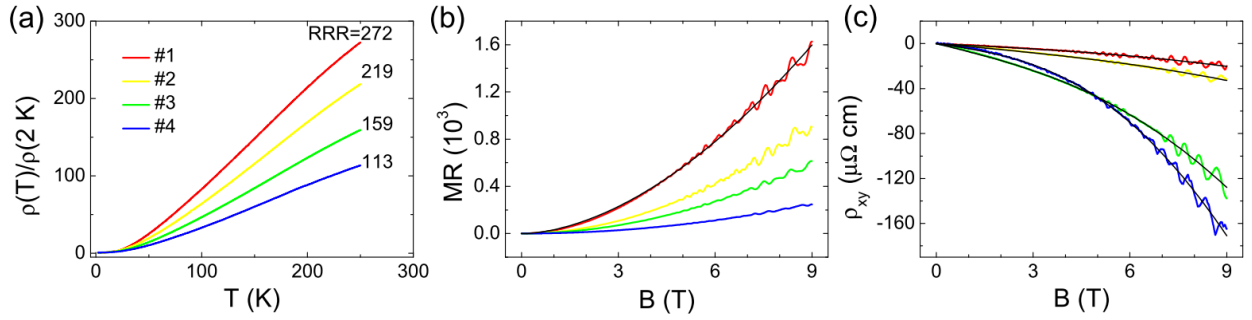


FIG. 2. (a) Temperature dependence of resistivity normalized by $\rho(2\text{ K})$ for samples #1, #2, #3 and #4, with the current applied along the *a* axis. Residual resistivity ratio (RRR), defined as $\rho(250\text{ K})/\rho(2\text{ K})$, is also presented. (b) Longitudinal magnetoresistance and (c) transverse Hall resistivity taken at 2 K in a field range of 0-9 T. Non-oscillatory curve in (b) represents the power-law fitting; non-oscillatory curves in (c) represent the fittings with the two-carrier model.

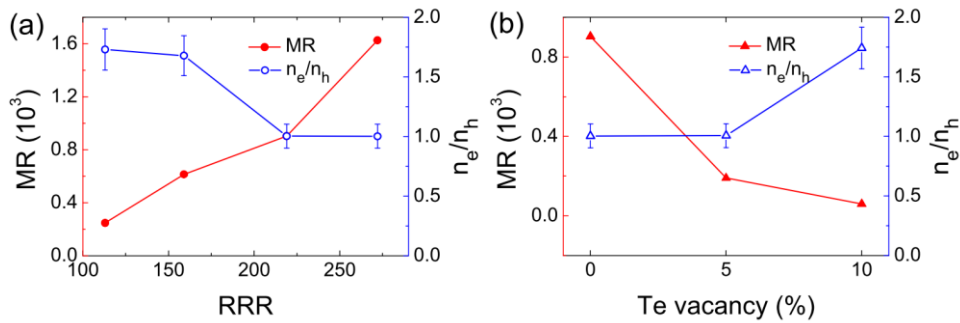


FIG. 3. (a) MR measured at 2 K and 9 T (filled circles) and the fitting-resultant n_e/n_h (open circles) as a function of RRR for the as-grown samples, obtained from Fig. 2. (b) MR (filled triangles) and n_e/n_h (open triangles) as a function of Te vacancy.

n_e/n_h (open triangles) as a function of Te vacancy for the annealed samples, obtained from Fig. 4.

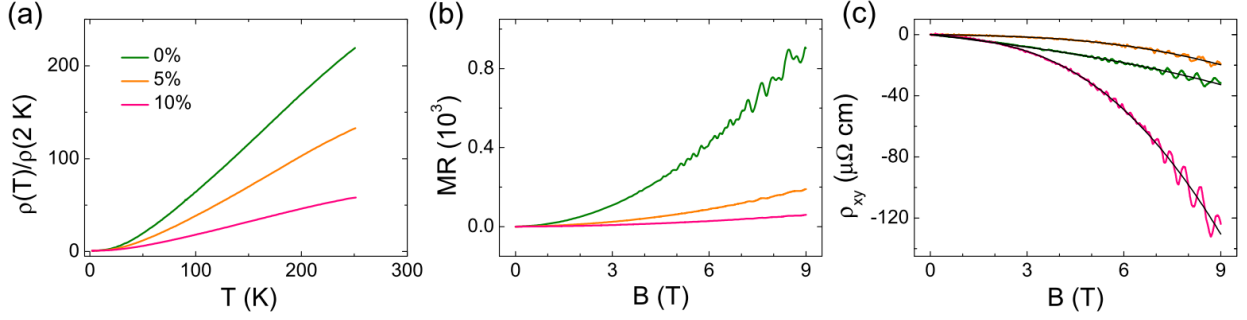


FIG. 4. (a) Temperature dependence of resistivity normalized by $\rho(2\text{ K})$ for the annealed samples with different Te vacancies. (b) Longitudinal magnetoresistance and (c) transverse Hall resistivity taken at 2 K in a field range of 0-9 T. Non-oscillatory curves represent the fittings with the two-carrier model.

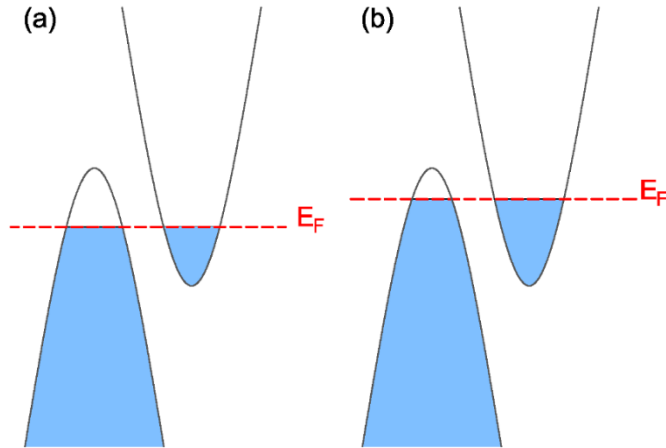


FIG. 5. Schematic illustration for the non-stoichiometry effect in WTe₂. Dashed lines indicate the Fermi level. Condition in (a) means perfect compensation of electron-type and hole-type carriers. (b) With electron doping, the electron-type carriers exceed the hole-type carriers. The less compensated ratio of n_e/n_h leads to a decrease in the XMR of WTe₂.